Band-structure pseudopotential calculation of zinc-blende and wurtzite AlN, GaN, and InN

Daniel Fritsch, Heidemarie Schmidt, and Marius Grundmann
Fakultät für Physik und Geowissenschaften, Institut für Experimentelle Physik II, Universität Leipzig, Linnéstrasse 3-5, 04103 Leipzig, Germany

(Received 23 October 2002; revised manuscript received 16 January 2003; published 26 June 2003)

The electronic properties of the zinc-blende and wurtzite group-III nitride compound semiconductors AlN, GaN, and InN are studied within the empirical pseudopotential approach. Using ionic model potentials and the static dielectric screening function derived by Levine and Louie [Z.H. Levine and St.G. Louie, Phys. Rev. B **25**, 6310 (1982)], the cationic and anionic model potential parameters were obtained from zinc-blende AlN, GaN, and InN experimental data. Exploiting the concept of transferable model potentials, we calculated the band structure of group-III nitrides in zinc-blende and wurtzite phase using the *same* ionic model potential parameters. Within this step we had to include the anisotropy of wurtzite crystals into the screening function. From the empirical fits for the effective masses at the Γ point, also a complete set of Luttinger and Luttinger-like $\mathbf{k}\cdot\mathbf{p}$ parameters has been extracted for zinc-blende and wurtzite nitrides, respectively.

DOI: 10.1103/PhysRevB.67.235205 PACS number(s): 71.15.Ap, 71.15.Dx, 71.20.Nr

I. INTRODUCTION

The great interest in the group-III nitride material system can be attributed to the promising electrical and optical properties of the binary compounds AlN, GaN, InN, and their alloys. These binary compounds usually crystallize in the wurtzite structure (α-nitrides). While the low-temperature direct band-gap energies of α-AlN (6.3 eV) (Refs. 1,2) and α-GaN (3.5 eV) (Refs. 3–5) are well known, various band gaps for lower-quality α-InN are projected in the broad energy range from 1.9 eV to 2.1 eV.[6–8] Measurements on single-crystalline α-InN samples recently obtained with an improved crystal-growth technique[9] yield a smaller fundamental band gap in the energy range from 0.7 eV to 1.0 eV.[10–12]

While the hexagonal wurtzite structure is the thermodynamically more stable modification, group-III nitrides can also be grown in the metastable cubic zinc-blende structure (β-nitrides), which possesses technological advantages such as easier doping, cleaving (for laser facets), and contacting.

With the band gaps of binary and ternary group-III nitrides spanning the whole visible region of the electromagnetic spectrum and the contiguous part of the ultraviolet (UV), one can think of optoelectronic devices working in the entire region from 200 nm to 1200 nm. Here the main focus is the short-wavelength laser diode for application in optical data storage systems and high-efficient light-emitting diodes working in the blue spectral region as the third primary color in semiconductor-based full color displays. Results of these researches are already to be seen in the availability of commercial blue laser diodes[13] and the realization of lasers working in the blue-violet spectral region for both pulsed[13,14] and continuous-wave[15] operations.

A number of theoretical and experimental studies of nitrides have been reported. In an early review Strite and Morkoç[16] discuss crystal-growth techniques as well as structural, optical, and electrical properties of AlN, GaN, InN, and their alloys. The technological importance of the group-III nitride material system for short-wavelength light-emitting devices was reviewed by Orton and Foxon.[17] A more recent review containing growth, characterization, and related properties was given by Jain *et al.*,[18] whereas a recent compilation given by Vurgaftman *et al.*[19] focuses on band parameters of III-V zinc-blende and wurtzite compound semiconductors thereby including the nitrides as well.

Band-structure calculations ranging from phenomenological methods such as the $\mathbf{k}\cdot\mathbf{p}$ theory to atomistic *ab initio* methods, such as the self-consistent full-potential linear augmented plane-wave method (FPLAPW) within local-density approximation (LDA), first-principles total-energy calculations, linear combination of atomic orbitals (LCAO) and pseudopotential methods, or more empirical methods such as the empirical pseudopotential method (EPM) have been performed. Being exactly in the description of the complete dispersion of the valence bands, first-principles methods have some well-known disadvantages.[20,21] On the other hand, the EPM yields the complete band dispersion of valence and conduction bands and reliably provides necessary band-structure parameters such as effective masses or equivalent $\mathbf{k}\cdot\mathbf{p}$ parameters of the zinc-blende and wurtzite phase nitrides for device modeling.

At present a majority of published works dealing with theoretically determined technologically important parameters of the nitride systems are based on the EPM (see Sec. II).

The aim of the present paper is to report about our detailed theoretical study of the electronic band structure for both zinc-blende and wurtzite group-III nitrides by means of the EPM approach. We make use of continuous ionic model potentials, which are screened by the model dielectric function $\varepsilon(q)$ derived for semiconductors by Levine and Louie.[22] We want to emphasize that this approach allows a continuous description in reciprocal space, the explicit inclusion of bond charges, and the exploitation of the ionic model potential transferability to other crystal structures, namely, the wurtzite crystal. Being capable of obtaining complete band dispersions, EPM supported by the concept of transferable model potentials is presently used to describe the electronic structure of alloys, superlattices, and other complex systems, e.g., quantum dots.[23] It should be noted that the transferability of

pseudopotential form factors, i.e., in the end of atomic model potentials, has been successfully demonstrated by Bergstresser and Cohen[24] for the more ionic ZnS. Also the most important conditions to be met by pseudopotentials, i.e., the transferability of the model potential and a continuous description in reciprocal space,[23] are formulated with regard to atomic model potentials without saying that the screening is different in various environments.

In this work we demonstrate the transferability of continuous, ionic model potentials taking into account the various environments by the dielectric screening function from Levine and Louie.[22] Furthermore, we will show by way of an example for wurtzite phase nitrides that crystal-specific anisotropies can be taken into account via the screening function $\varepsilon(q)$. Within this method we calculated a set of effective masses or Luttinger and Luttinger-like $\mathbf{k}\cdot\mathbf{p}$ parameters for zinc-blende nitrides and wurtzite nitrides, respectively. We find an overall agreement with other published results and show once more that the stated disadvantage of the initial EPM calculations of giving poor effective masses[23] does not apply to the model potential parameters used in the present work.

This paper is organized as follows. In Sec. II the concept of transferable model potentials is exploited for two different crystal structures, namely, for the zinc-blende and wurtzite modification and the results of EPM electronic band-structure calculations are given at high-symmetry points. In Sec. III we review the use of $\mathbf{k}\cdot\mathbf{p}$ theory and extract the $\mathbf{k}\cdot\mathbf{p}$ parameters from the calculated band structures. A summarizing conclusion will end this paper.

II. EPM CALCULATIONS

Numerous results of band-structure calculations on zinc-blende and wurtzite phase group-III nitrides can be found in the literature. There are self-consistent FPLAPW calculations on β-nitrides,[25] α-AlN,[21] and α-GaN,[21,26] LCAO calculations on α-AlN and α-GaN[27] as well as full-potential linear muffin-tin orbital (LMTO) calculations on the α- and β-phases of AlN and GaN.[28] The majority of published works dealing with technologically important parameters of the nitride systems are based on the EPM. For example, pseudopotential calculations based on different model potentials can be found for α-AlN,[29–32] α-GaN,[29–34] α-InN,[30–32,34] β-AlN,[20,29,35] β-GaN,[20,29,33,35,36] and for β-InN.[36]

The present work will provide the EPM electronic band-structure as well as corresponding sets of $\mathbf{k}\cdot\mathbf{p}$ parameters for AlN, GaN, and InN, in both crystal modifications. To the best of our knowledge there exist no other EPM investigations of group-III nitrides AlN, GaN, and InN where the Al, Ga, In, and N model potentials are the *same* for both zinc-blende and wurtzite crystals. The employed EPM approximations will be briefly discussed in Sec. II A. In Secs. II B and II C we report on the crystal-specific implementations of the EPM and the results of our band-structure calculations for β-nitrides and α-nitrides, respectively.

A. Empirical pseudopotential method

The starting point for any pseudopotential calculation is the pseudo-wave-equation

$$\left[-\frac{\hbar^2}{2m_0}\Delta + V^{\text{pseudo}}(\mathbf{r})\right]\psi_{\text{n}}(\mathbf{k},\mathbf{r}) = E_{\text{n}}(\mathbf{k})\,\psi_{\text{n}}(\mathbf{k},\mathbf{r}), \quad (1)$$

which follows from simplifying the many-particle Schrödinger equation. $V^{\text{pseudo}}(\mathbf{r})$ is the pseudopotential that possesses the crystal symmetry and fulfills $V^{\text{pseudo}}(\mathbf{r}) = V^{\text{pseudo}}(\mathbf{r}+\mathbf{R})$, where $\mathbf{R}$ is a lattice vector.

The intuitive ansatz for $V^{\text{pseudo}}(\mathbf{r})$ involves a sum over spherically symmetric atomic model potentials:

$$V^{\text{pseudo}}(\mathbf{r}) = \sum_{\mathbf{r}_\nu} V_{a\nu}(\mathbf{r}-\mathbf{r}_\nu), \quad (2)$$

where a represents different types of atoms located at the atomic sites $\mathbf{r}_\nu$. The valence electrons are assumed to move nearly free in the weak one-electron potential. Therefore, the pseudo-wave-function can be expanded in terms of a linear combination of plane waves $[PW(\mathbf{k},\mathbf{r})]$:

$$\psi(\mathbf{k},\mathbf{r}) = \sum_{\text{i}} c_{\text{i}}(\mathbf{k})\,PW(\mathbf{k}+\mathbf{G},\mathbf{r}), \quad (3)$$

which satisfy Bloch's theorem. Here $\mathbf{G}$ denotes a reciprocal lattice vector. The energy-band dispersion $E_{\text{n}}(\mathbf{k})$, and the expansion coefficients $c_{\text{i}}(\mathbf{k})$ in Eq. (3) are obtained from the relevant secular equation:

$$\left\| \left(\frac{\hbar^2}{2m_0}|\mathbf{k}+\mathbf{G}|^2 - E\right)\delta_{\mathbf{G},\mathbf{G}'} + \sum_{\mathbf{r}_\nu} e^{-i(\mathbf{G}-\mathbf{G}')\mathbf{r}_\nu} V_{a\nu}(\mathbf{G}-\mathbf{G}') \right\| = 0. \quad (4)$$

The Fourier transform of the atomic model potential $V_{a\nu}(\mathbf{G}-\mathbf{G}')$ in Eq. (4) only contains information on the constitutive atoms and is known as the pseudopotential form factor. The term $e^{-i(\mathbf{G}-\mathbf{G}')\mathbf{r}_\nu}$ describes the structural arrangement of the atoms in the crystal and is known as the structure factor, which can be found for different crystal structures, e.g., in Ref. 37.

B. Electronic properties of β-nitrides

Usually for the explicit form of the atomic model potential adjustable parameters are used, either in an *ab initio* or atomic model potential approach.

In this work we make use of ionic empty-core potentials for the local ionic cation ($i=c$) and the local ionic anion ($i=a$), which are given in atomic units ($\hbar^2 = e^2/2 = 2m_0 = 1$) by

$$V_{\text{ionic}}(r) = \begin{cases} 0 & \text{for} \quad r < r_i \\ -\dfrac{2z_i}{r} & \text{for} \quad r > r_i, \end{cases} \quad (5)$$

where the adjustable parameters z_i and r_i correspond to an effective charge and an effective core radius, respectively. We obtain the expression for the atomic pseudopotential

TABLE I. Experimental values of β-nitrides used in the fitting procedure.

	AlN	GaN	InN
a(nm)	0.438[a]	0.452[b]	0.498[c]
ε_0	9.56[d]	9.55[e]	12.45[f]
E_{gap} (eV)	5.34[g](X)	3.302[h](Γ)	2.11[i](Γ)
Δ_0 (meV)	19[j]	17[h]	6[j]

[a]Experimental value from Ref. 39.
[b]Experimental value from Ref. 42.
[c]Experimental value from Ref. 45.
[d]Averaged from the values $\varepsilon_0^{\perp}=9.0$ and $\varepsilon_0^{\parallel}=10.7$ for α-AlN from Ref. 40.
[e]Averaged from the values $\varepsilon_0^{\perp}=9.28$ and $\varepsilon_0^{\parallel}=10.1$ for α-GaN from Ref. 43.
[f]Averaged from the values $\varepsilon_0^{\perp}=9.82$ and $\varepsilon_0^{\parallel}=17.71$ for α-InN from Ref. 46.
[g]Experimental value from Ref. 41.
[h]Experimental value from Ref. 44.
[i]Experimental value from Ref. 8.
[j]Recommended value from Ref. 19.

$V(\mathbf{q})$, where $\mathbf{q}=|\mathbf{G}-\mathbf{G}'|$, by screening the Fourier transform of the ionic model potential:

$$V(q)=\frac{V_{\text{ionic}}(q)}{\varepsilon(q)}, \tag{6}$$

where $\varepsilon(q)$ is the static limit of the model dielectric function, which has been derived for semiconductors by Levine and Louie[22] as follows:

TABLE II. Fitting parameters of the ionic model potential as defined in Eq. (5). The small variation in the N-potential parameters r_a and z_a is attributed to the approximated β-nitride ε_0-values and the fixed bond charge position midway between the atoms.

	AlN	GaN	InN
r_c	1.3143	1.0242	1.1009
r_a	0.6569	0.6729	0.6698
z_c	3.5198	3.5582	3.8674
z_a	6.0253	6.0015	5.9945

$$\varepsilon(q)=1+\frac{1}{L^2q^2}\left\{\frac{1}{2}-\frac{\lambda}{4z}\left[\tan^{-1}\left(\frac{y_+}{\lambda}\right)+\tan^{-1}\left(\frac{y_-}{\lambda}\right)\right]+\left(\frac{\lambda^2}{16z^3}+\frac{1}{4z}-\frac{z}{16}\right)\ln\left(\frac{\lambda^2+y_+^2}{\lambda^2+y_-^2}\right)\right\}, \tag{7}$$

with $z=q/\mathbf{k}_F$ and $y_{\pm}=z(2\pm z)$. $\mathbf{k}_F$ is the Fermi wave vector and $L^2=\pi/4\mathbf{k}_F$ denotes the square of the Thomas-Fermi screening length in atomic units. The parameter

$$\lambda=\frac{2}{\sqrt{3L^2\mathbf{k}_F^2(\varepsilon_0-1)}} \tag{8}$$

fulfills the boundary condition $\varepsilon(q=0)=\varepsilon_0$.

In order to obtain the adjustable parameters z_i and r_i of the ionic model potentials for the Al, Ga, and In cations and the N anion, we limited the expansion of $\psi_n(\mathbf{k},\mathbf{r})$ in plane waves to reciprocal wave vectors with $|\mathbf{G}|<\sqrt{20}(2\pi/a)$, where a is the lattice constant of the zinc-blende lattice. The cationic model potential parameters for Al, Ga, and In were already known from an earlier work[38] on arsenides and phosphides and served as start parameters in a Levenberg-

TABLE III. Zinc-blende AlN, GaN, and InN energies at high-symmetry points in eV. All values refer to the top of the valence band. The labeling of the energy-bands is given for calculations where spin-orbit effects are neglected (included).

Ref.		AlN		GaN			InN	
		This work	[a]	This work	[a]	[b]	This work	[b]
Γ_{15}^c	(Γ_7^c)	12.579	13.406	10.098	10.300	10.248	9.722	10.193
Γ_1^c	(Γ_6^c)	5.840	5.936	3.308	3.383	3.213	2.112	1.939
Γ_{15}^v	(Γ_8^v)	0.000	0.000	0.000	0.000	0.000	0.000	0.000
X_3^c	(X_7^c)	8.794	10.661	6.010	6.805	6.265	6.416	7.392
X_1^c	(X_6^c)	5.346	5.102	4.428	4.571	4.585	5.187	2.509
X_5^v	(X_7^v)	−2.315	−2.337	−2.459	−2.693	−2.086	−1.555	−1.408
X_3^v	(X_6^v)	−5.388	5.262	−6.294	−6.149	−5.923	−4.303	−4.400
L_3^c	($L_{4,5}^c$)	12.202	12.014	10.416	9.916	10.606	10.168	8.060
L_1^c	(L_6^c)	8.264	9.423	5.149	5.636	5.510	4.733	5.818
L_3^v	($L_{4,5}^v$)	−0.718	−0.728	−0.834	−0.931	−0.772	−0.480	−0.456
L_2^v	(L_6^v)	−6.251	−6.179	−6.812	−6.743	−6.644	−4.667	−5.200

[a]Empirical pseudopotential calculation from Ref. 20.
[b]Empirical pseudopotential calculation from Ref. 36.

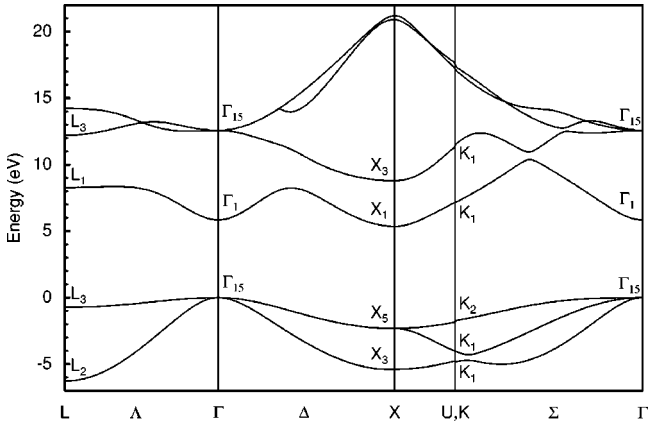

FIG. 1. Band structure of β-AlN along high-symmetry lines in the Brillouin zone.

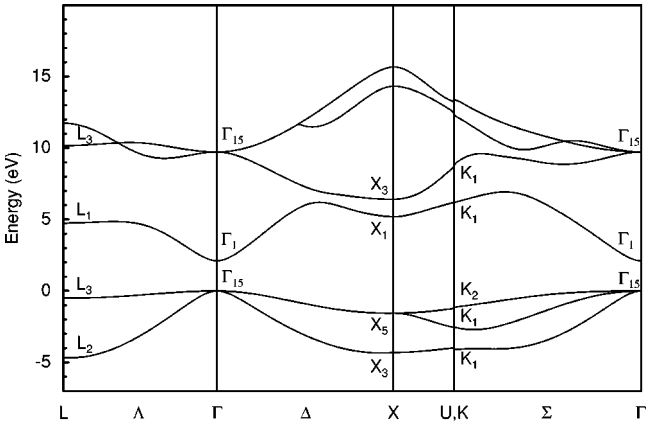

FIG. 3. Band structure of β-InN along high-symmetry lines in the Brillouin zone.

Marquardt fitting procedure where the cationic and anionic potential parameters were varied in order to obtain closest agreement between the calculated band-structures and experimental low-temperature transition energies of AlN, GaN, and InN. The experimental values used in the fitting procedure $(a,\varepsilon_0,E_{\mathrm{gap}},\Delta_0)$ and in the band-structure calculation $(a,\varepsilon_0,\Delta_0)$ are given in Table I. The ε_0 values for β-nitrides are approximated from well-known experimentally determined α-nitride ε_0 values via $\tilde{\varepsilon}_0=\frac{1}{3}(2\varepsilon_0^{\perp}+\varepsilon_0^{\parallel})$. The three sets of model parameters z_i and r_i resulting from separate fits of the binary nitrides AlN, GaN, and InN are given in Table II. As can be seen, the variation in the N-potential parameters is very small ($\sim 1\%$). However, we attribute this to the fact that we had to approximate the β-nitride ε_0 values and that we have kept the position of the bond charges fixed midway between the atoms in our band-structure calculations, i.e., the different ionicities of β-nitrides have not been taken into account by a shift of the bond charge position toward the N anion in more ionic β-nitrides.

Making use of the fitted parameters we calculated the energy-band dispersion $E_{\mathrm{n}}(\mathbf{k})$ of AlN, GaN, and InN by means of Eq. (4). The resulting transition energies at high-symmetry points in comparison to other published results are given in Table III. As can be seen, the fitted band-structures well reproduce the known experimental band gaps (Table I) within a few meV.

We compared our results with band-structure calculations where the spin-orbit splitting was included (see Table III) though the spin-orbit splitting energy is small for β-nitrides. The corresponding labeling of the energy bands is given within parenthesis in Table III. Besides some higher transition energies, our results compare well with the other published results.

The corresponding band-structures along the main symmetry lines in the Brillouin zone are given in Figs. 1–3.

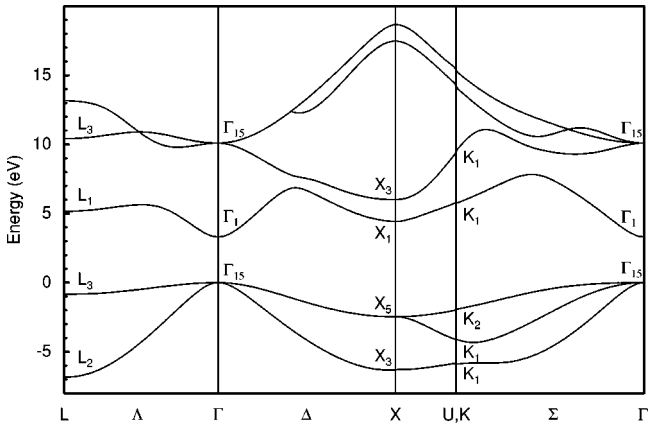

FIG. 2. Band structure of β-GaN along high-symmetry lines in the Brillouin zone.

C. Electronic properties of α-nitrides

Making use of the model potential parameters obtained from β-nitrides, we intend to determine the energy-band dispersion of the wurtzite phase nitrides as well. For this we

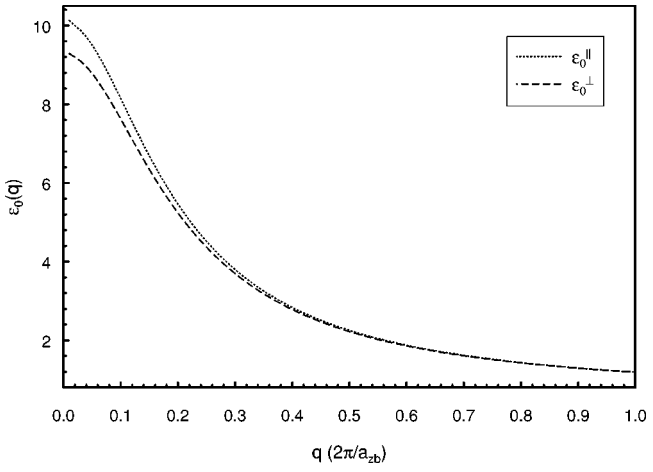

FIG. 4. Direction dependent screening function $\varepsilon(q)$ calculated by means of Eq. (7) using experimental data of α-GaN ($\varepsilon_0^{\perp}=9.28$ and $\varepsilon_0^{\parallel}=10.1$) (Ref. 43). The smallest reciprocal lattice vector q_{s} of α-GaN and β-GaN lies at $q_{\mathrm{s}}^{\alpha}=(\sqrt{3}/2)(2\pi/a_{\mathrm{zb}})$ and $q_{\mathrm{s}}^{\beta}=\sqrt{3}(2\pi/a_{\mathrm{zb}})$, respectively.

TABLE IV. Wurtzite AlN, GaN, and InN critical-point transition energies in eV. The mark aniso describes the values obtained by a band-structure calculation using anisotropically screened model potentials, whereas the mark iso describes a comparative band-structure calculation based on isotropically screened model potentials using an averaged ε_0 value by taking the spur of the dielectric tensor.

Ref.	AlN				GaN					InN			
	This work		[a]	[b]	This work		[a]	[c]	[d]	This work		[e]	[d]
	Aniso	Iso		Expt	Aniso	Iso			Expt	Aniso	Iso		Expt
$M_2^v-M_1^c$	9.56	9.54	10.0		7.67	7.67	8.26		7.05	7.30	7.23	6.65	7.3,4.95 [f]
$M_4^v-M_1^c$	7.88	7.87	8.3		6.07	6.07	6.61		7.0[g]	5.94	5.88	5.05	
$M_4^v-M_3^c$	8.81	8.83	8.5		7.68	7.68	7.69		7.05	6.71	6.70	5.80	7.3
$\Gamma_6^v-\Gamma_1^c$	6.11	6.11	6.0	6.29	3.47	3.47	3.50	3.0	3.6,3.44[g],3.50[g]	2.58	2.59	2.04	2.11,2.0 [f,h]
$\Gamma_3^v-\Gamma_6^v$	6.44	6.41	6.7		6.97	6.94	6.80	7.0	7.0[g]	5.63	5.50	5.77	
$\Gamma_1^v-\Gamma_6^v$	0.13	0.16	0.2		0.043	0.023	0.021	0.0	0.022[g]	0.214	0.084	0.017	
$\Gamma_5^v-\Gamma_6^v$	1.04	1.03	0.9		1.00	1.00		1.0		0.90	0.89	1.05	
$\Gamma_5^v-\Gamma_3^c$	8.95	8.94	9.4	8.02	5.96	5.96		5.9	5.3	5.22	5.18	4.65	5.0,5.5,4.7 [f]
$\Gamma_5^v-\Gamma_6^c$	12.99	12.97	14.0	14.00	10.74	10.74		11.1	9.4	10.16	10.12	8.74	8.8,8.9 [f]
$H_3^v-H_3^c$	10.10	10.91	10.5	10.39	8.06	8.07	9.0		7.9[g]	7.34	7.36	6.51	5.4 [f]
$K_3^v-K_2^c$	9.43	9.43	9.6		8.54	8.55	9.43	8.3	7.65,9.0[g]	8.13	8.12	7.38	7.3,7.2 [f]
$K_2^v-K_2^c$	9.59	9.57	9.7		8.68	8.68	10.10	7.9		8.60	8.50	7.20	

[a] *Ab initio* pseudopotential calculation within local-density approximation from Ref. 29.
[b] Experimental values taken from Ref. 2.
[c] LCAO within local-density approximation from Ref. 47.
[d] If not quoted otherwise, the experimental values are taken from Ref. 48.
[e] Empirical pseudopotential calculation from Ref. 34.
[f] Experimental values taken from Ref. 8.
[g] Experimental values taken from Ref. 34.
[h] For a detailed discussion of the calculated α-InN fundamental band gap in comparison to the recently measured experimental band gaps in the energy range of 0.7–1.0 eV (Refs. 10–12) we refer to Sec. II C.

exploit the concept of transferable model potentials. This concept traces back to the work by Bergstresser and Cohen.[24] They fitted the atomic potential form factors $V(\mathbf{q})$ at discrete, allowed reciprocal lattice vectors to experimentally determined excitation energies. Later on, by introducing continuous atomic potentials and fitting the adjustable model potential parameters to reproduce experimental data, the reliability of such model potentials could be strongly enhanced. In the present work we even go a step further by using continuous ionic model potentials that describe only the core of the atoms. Within this concept, we take care of various environments via a direction-dependent screening function, e.g., we are able to incorporate the wurtzite-type lattice anisotropies in our calculations.

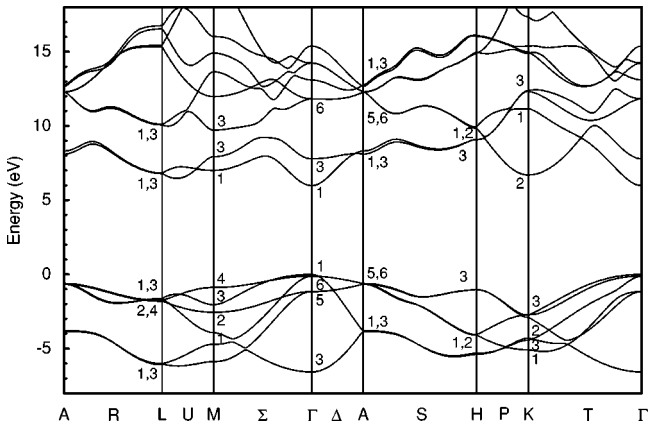

FIG. 5. Band structure of α-AlN along high-symmetry lines in the Brillouin zone.

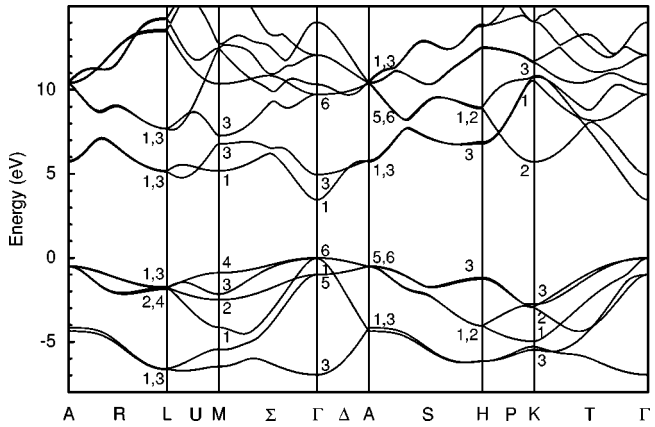

FIG. 6. Band structure of α-GaN along high-symmetry lines in the Brillouin zone.

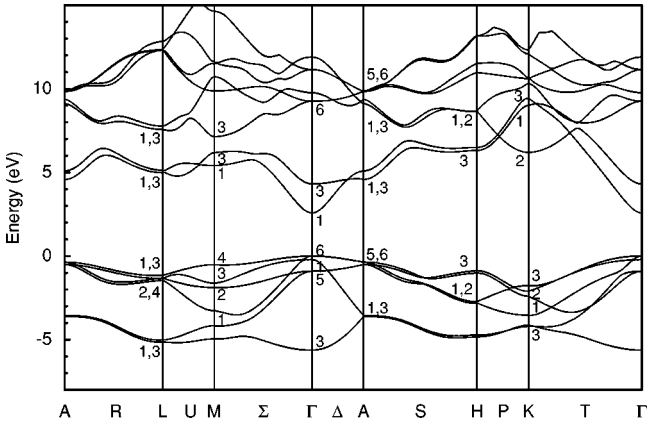

FIG. 7. Band structure of α-InN along high-symmetry lines in the Brillouin zone.

The transferability in the present work is assured because the spherically symmetric model potentials used in the present work are independent of structural influences. The arrangement of the atoms in the wurtzite crystal is reflected by the structure factors of the wurtzite lattice.[37] A closer look at the model dielectric screening function $\varepsilon(q)$ reveals an implicit direction dependence of $\varepsilon(q)$ for screening ionic model potentials, for example, in a wurtzite structure. This direction dependence enters $\varepsilon(q)$ via parameter λ, which implies the finite dielectric constant ε_0 of the compound semiconductor. In wurtzite crystals, two values $\varepsilon_0^{\perp}$ and $\varepsilon_0^{\parallel}$, i.e., the static dielectric constant in the (k_x,k_y) plane perpendicular and parallel to the main crystal axis *c*, respectively, imply a small anisotropy of the wurtzite structure and, according to Eq. (7), two different screening functions $\varepsilon^{\perp}(q)$ and $\varepsilon^{\parallel}(q)$.

As can be seen in Fig. 4, the difference between $\varepsilon^{\perp}(q)$ and $\varepsilon^{\parallel}(q)$ is the largest for small q values. This will be of great importance for modeling the properties of crystals with large unit cells because the magnitude of the smallest allowed reciprocal lattice vector decreases with increasing unit-cell size.

To correctly screen the ionic model potential, we use the vector representation of the reciprocal lattice vector $\mathbf{q}$ entering Eq. (6). Taking the vector component $\mathbf{q}_{\perp}$ in the (k_x,k_y) plane and $\mathbf{q}_{\parallel}$ parallel to the *c* axis, we obtain a direction-dependent vector notation of $\mathbf{q}$ $(\mathbf{q}=\mathbf{q}_{\perp}+\mathbf{q}_{\parallel})$. With it, the screening of the ionic model potential now depends not only on the absolute value q but also on the direction-dependent $\varepsilon(q)$:

$$\varepsilon(q)=\frac{\varepsilon_0^{\perp}q_{\perp}^2+\varepsilon_0^{\parallel}q_{\parallel}^2}{\mathbf{q}^2}. \tag{9}$$

The resulting transition energies at high-symmetry points in comparison to other published results are given in Table IV. Keeping in mind that we used the model potential parameters obtained from a fit to the scarce experimental data available for β-nitrides, the agreement between our band-structure calculation and both, other theoretical as well as available experimental data for α-nitrides is quite good.

One exception we would like to make in the case of α-InN. Making use of the model potential parameters obtained from the β-InN experimental data and calculating the α-InN band-structure by exploiting the transferability of the pseudopotential form factors, we reproduce the experimental value of 2.11 eV, which is accepted as the InN fundamental energy gap. Recalling recent works that place the α-InN band gap in the energy range below 1 eV,[10–12] and the α-nitride band gaps being at most 20% larger than the corresponding β-nitride band gaps, we predict that the β-InN fundamental energy gap has to be corrected to an energy value below 0.8 eV. This assumption is supported by the fact that the band-structures for α-AlN and α-GaN calculated using the same method give reliable results in agreement with other calculations and experimental data.

The corresponding band-structures along the main symmetry lines in the Brillouin zone are given in Figs. 5–7. As will be shown in Sec. III B in detail, the anisotropy influences the transition energies and the effective masses mainly at the Γ point.

The explicit consideration of structural anisotropies via a direction-dependent screening function is the great advantage of the ionic model potential used in this work compared to plain atomic model potentials and will also be very useful for modeling crystals with large unit cells.

III. DERIVATION OF EFFECTIVE-MASS PARAMETERS

A. Effective-mass approximation of β-nitrides

As we are interested in extracting the Luttinger parameters γ_i and the conduction- and valence-band effective

TABLE V. Luttinger parameters γ_1, γ_2, and γ_3 for zinc-blende AlN, GaN, and InN obtained from a fit along the [110] direction and literature data.

	AlN					GaN					InN	
Ref.	This work	a	b	c	d	This work	a	b	c	d	This work	d
γ_1	1.85	1.54	1.50	1.91	1.92	2.89	2.96	2.70	3.07	2.67	2.78	3.27
γ_2	0.43	0.42	0.39	0.48	0.47	0.85	0.90	0.76	0.86	0.75	0.97	1.26
γ_3	0.74	0.64	0.62	0.74	0.85	1.20	1.20	1.07	1.26	1.10	1.22	1.63

[a]Self-consistent FPLAPW method within local-density approximation from Ref. 25.
[b]First-principles band-structure calculations from Ref. 50.
[c]Empirical pseudopotential calculation from Ref. 35.
[d]Recommended values taken from Ref. 19.

masses of the zinc-blende nitrides, we have to couple the results of our band-structure calculations with effective-mass theory. The *s*-like conduction-band effective mass can be obtained through a simple parabolic fit using the definition of the effective mass as the second derivative of the energy band with respect to wave vector **k** via

$$\left(\frac{m_0}{m^*}\right)=\left(-\frac{m_0}{\hbar^2}\right)\left(\frac{\partial^2 E}{\partial k^2}\right). \tag{10}$$

The valence-band states of the Γ point are derived from *p*-bonding states due to the tetrahedral coordination in zinc-blende crystals. Taking into account the three highest-lying valence bands, the basis of Bloch states for the corresponding $\mathbf{k}\cdot\mathbf{p}$ model consists of the six angular momentum eigenstates $|jm_j\rangle$, where $j=\frac{3}{2}$, $m=\pm\frac{3}{2},\pm\frac{1}{2}$ corresponds to the four Γ_8 heavy- and light-hole valence-band states and $j=\frac{1}{2}$, $m=\pm\frac{1}{2}$ corresponds to the two Γ_7 spin-orbit split-off valence-band states. The Γ_8 and Γ_7 eigenvalues are separated by Δ_{so} due to spin-orbit interaction. To describe the valence-band-structure, we adopt the effective-mass Hamiltonian derived by Luttinger and Kohn using $\mathbf{k}\cdot\mathbf{p}$ theory.[49] The resulting $\mathbf{k}\cdot\mathbf{p}$ matrix with zinc-blende symmetry can be written as[25]

$$\begin{pmatrix}
Q & S & R & 0 & \frac{i}{\sqrt{2}}S & -i\sqrt{2}R \\
S^* & T & 0 & R & -\frac{i}{\sqrt{2}}(Q-T) & i\sqrt{\frac{3}{2}}S \\
R^* & 0 & T & -S & -i\sqrt{\frac{3}{2}}S^* & -\frac{i}{\sqrt{2}}(Q-T) \\
0 & R^* & -S^* & Q & -i\sqrt{2}R^* & -\frac{i}{\sqrt{2}}S^* \\
-\frac{i}{\sqrt{2}}S^* & \frac{i}{\sqrt{2}}(Q-T) & i\sqrt{\frac{3}{2}}S & i\sqrt{2}R & \frac{1}{2}(Q+T)-\Delta_{so} & 0 \\
i\sqrt{2}R^* & -i\sqrt{\frac{3}{2}}S^* & \frac{i}{\sqrt{2}}(Q-T) & \frac{i}{\sqrt{2}}S & 0 & \frac{1}{2}(Q+T)-\Delta_{so}
\end{pmatrix}, \tag{11}$$

where

$$Q=-\frac{\hbar^2}{2m_0}[(\gamma_1+\gamma_2)(k_x^2+k_y^2)+(\gamma_1-2\gamma_2)k_z^2],$$

$$T=-\frac{\hbar^2}{2m_0}[(\gamma_1-\gamma_2)(k_x^2+k_y^2)+(\gamma_1+2\gamma_2)k_z^2],$$

$$S=i\frac{\hbar^2}{m_0}\sqrt{3}\gamma_3(k_x-ik_y)k_z,$$

$$R=-\frac{\hbar^2}{2m_0}\sqrt{3}[\gamma_2(k_x^2-k_y^2)-2i\gamma_3k_xk_y], \tag{12}$$

m_0 denotes the free electron mass, and γ_1, γ_2, and γ_3 are the Luttinger parameters.

Solving for the eigenvalues of the $\mathbf{k}\cdot\mathbf{p}$ matrix without spin-orbit interaction ($\Delta_{so}=0$) along the [110] direction yields analytical expressions for the three highest spin-degenerate valence bands E_1, E_2, and E_3 in dependence on the Luttinger parameters γ_i:

$$E_1=-\frac{\hbar^2}{2m_0}(-\gamma_1-\gamma_2+3\gamma_3)k^2,$$

$$E_2=-\frac{\hbar^2}{2m_0}(-\gamma_1+2\gamma_2)k^2,$$

$$E_3=-\frac{\hbar^2}{2m_0}(-\gamma_1-\gamma_2-3\gamma_3)k^2. \tag{13}$$

Calculating the [110] band dispersion near the Γ point with a high **k**-point density, we are able to fit the Luttinger parameters directly to the three valence bands. The results of these fits by means of Eq. (13) are given in Table V.

In order to obtain the valence-band effective masses, we have solved for the eigenvalues of the $\mathbf{k}\cdot\mathbf{p}$ matrix taking spin-orbit interaction into account. We have obtained the following analytical expressions for direction-dependent effective masses in dependence on the Luttinger parameters:

TABLE VI. Effective masses for electrons (e), heavy-holes (hh), light-holes (lh), and spin-orbit split-off-holes (so) in units of the free electron mass m_0 along the [100], [111], and [110] directions for zinc-blende AlN, GaN, and InN.

	Ref.	m_e	$m_{hh}^{[100]}$	$m_{lh}^{[100]}$	$m_{hh}^{[111]}$	$m_{lh}^{[111]}$	$m_{hh}^{[110]}$	$m_{lh}^{[110]}$	m_{so}
AlN									
	This work	0.23	1.02	0.37	2.64	0.30	1.89	0.32	0.54
	[a]	0.28	1.44	0.42	4.24	0.36	3.03	0.37	0.63
	[b]	0.21	1.05	0.35	2.73	0.30	2.16	0.31	0.51
	[c]	0.30	1.39	0.44	3.85	0.36	2.67	0.38	0.67
	[d]	0.25	1.02	0.35	4.55	0.28	2.44	0.29	0.47
GaN									
	This work	0.14	0.84	0.22	2.07	0.19	1.52	0.20	0.35
	[a]	0.14	0.86	0.21	2.09	0.19	1.65	0.19	0.30
	[b]	0.13	0.76	0.21	1.93	0.18	1.51	0.19	0.32
	[c]	0.17	0.85	0.24	1.79	0.21	1.40	0.21	0.37
	[d]	0.15	0.85	0.24	2.13	0.21	1.55	0.21	0.29
	[e]	0.12	1.34	0.70	1.06	0.63	1.44	0.58	0.20
InN									
	This work	0.13	1.18	0.21	2.89	0.19	2.12	0.20	0.36
	[d]	0.12	0.83	0.16	0.83	0.16	1.55	0.15	0.30
	[e]	0.10	2.18	0.89	2.29	0.93	3.10	0.79	0.30

[a]Self-consistent FPLAPW method within local-density approximation from Ref. 25.
[b]Empirical pseudopotential calculation from Ref. 35.
[c]Calculated from Luttinger parameters from Ref. 50 using Eqs. (14) and (15).
[d]Calculated from recommended Luttinger parameters from Ref. 19 using Eqs. (14) and (15).
[e]Empirical pseudopotential calculation from Ref. 36.

$$\left(\frac{m_0}{m^*_{hh/lh}}\right)^{[100]} = \gamma_1 \mp 2\gamma_2,$$

$$\left(\frac{m_0}{m^*_{hh/lh}}\right)^{[111]} = \gamma_1 \mp 2\gamma_3,$$

$$\left(\frac{m_0}{m^*_{hh/lh}}\right)^{[110]} = \frac{1}{2}(2\gamma_1 \mp \gamma_2 \mp 3\gamma_3), \tag{14}$$

where indices hh and lh denote the heavy-hole and light-hole effective masses, respectively. The spin-orbit split-off-hole (so) effective mass is isotropically in the three directions and is given by

$$\left(\frac{m_0}{m^*_{so}}\right) = \gamma_1. \tag{15}$$

The fitted hh, lh, so, and e effective masses and published results from other groups are given in Table VI.

As can be seen, the electron effective mass for β-GaN is in agreement with the experimental value of 0.15 ± 0.01 as given by Fanciulli *et al.*[51] The calculated electron effective masses of β-AlN (β-InN) 0.23 (0.13) are in agreement with the recommended values of 0.25 (0.12) as given in the review by Vurgaftman *et al.*[19]

B. Effective-mass approximation of α-nitrides

To derive the Luttinger-like parameters A_i and the valence- and conduction-band effective masses of wurtzite phase nitrides, we make use of the effective-mass Hamiltonian in the cubic approximation as given by Suzuki *et al.*:[21]

$$H = \begin{pmatrix} F & 0 & -H^* & 0 & K^* & 0 \\ 0 & G & \Delta & -H^* & 0 & K^* \\ -H & \Delta & \lambda & 0 & I^* & 0 \\ 0 & -H & 0 & \lambda & \Delta & I^* \\ K & 0 & I & \Delta & G & 0 \\ 0 & K & 0 & I & 0 & F \end{pmatrix}, \tag{16}$$

where F, G, H, I, K, Δ, λ, and θ are defined as

$$F = \Delta_1 + \Delta_2 + \lambda + \theta,$$

$$G = \Delta_1 - \Delta_2 + \lambda + \theta,$$

$$H = iA_6k_z(k_x + ik_y) - A_7(k_x + ik_y),$$

$$I = iA_6k_z(k_x + ik_y) + A_7(k_x + ik_y),$$

$$K = A_5(k_x + ik_y)^2,$$

$$\Delta = \sqrt{2}\Delta_3,$$

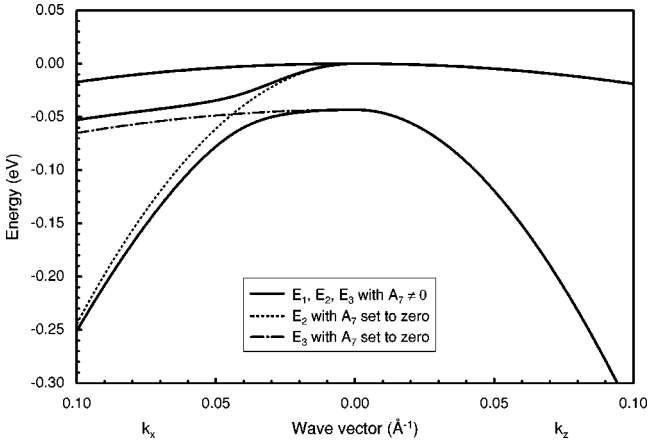

FIG. 8. Valence-band structure of α-GaN near the Γ point calculated by means of anisotropically screened model potentials. The valence bands E_1, E_2, and E_3 in the k_x and k_z directions can exactly be fitted using Eq. (18).

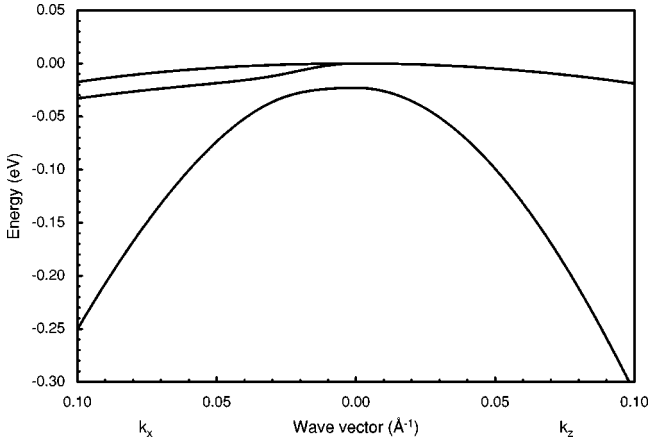

FIG. 9. Valence-band structure of α-GaN near the Γ point calculated by means of isotropically screened model potentials. Note the smaller crystal-field splitting in comparison to anisotropically screened model potentials (Fig. 8).

$$\lambda = A_1 k_z^2 + A_2(k_x^2 + k_y^2),$$

$$\theta = A_3 k_z^2 + A_4(k_x^2 + k_y^2). \tag{17}$$

Here Δ_1 corresponds to the crystal-field splitting energy, Δ_2 and Δ_3 account for the spin-orbit interaction via $\Delta_2 = \Delta_3 = \frac{1}{3}\Delta_{so}$. k_i represents the wave vector and A_i are the Luttinger-like parameters.

Without spin-orbit interaction, the energy-band dispersion of the $\mathbf{k}\cdot\mathbf{p}$ Hamiltonian ($\Delta_2 = \Delta_3 = 0, F = G, \Delta = 0$) simplifies to

$$E_1 = F' - K',$$

TABLE VII. Effective masses in units of free electron mass m_0, Luttinger-like parameters A_i ($i = 1, \ldots, 6$) in units of $\hbar^2/2m_0$, and A_7 in units of eV Å for wurtzite phase AlN. The crystal-field splitting energy Δ_1 is given in units of meV.

Ref.	This work		[a]	[b]	[c]	[d]	[e]	[f]
	Aniso	Iso						
$m_e^{\parallel}$	0.231	0.232	0.33	0.33	0.24	0.24	0.35	0.33
$m_e^{\perp}$	0.242	0.242	0.25	0.25	0.25	0.25		
$m_{hh}^{\parallel}$	2.370	2.382	3.68	3.53	1.949	1.869	3.53	4.41
$m_{lh}^{\parallel}$	2.370	2.382	3.68	3.53	1.949	1.869	3.53	4.41
$m_{ch}^{\parallel}$	0.209	0.209	0.25	0.25	0.229	0.212	0.26	0.27
$m_{hh}^{\perp}$	3.058	3.040	6.33	10.42	2.584	2.421	11.14	2.18
$m_{lh}^{\perp}$	0.285	0.287	0.25	0.24	0.350	0.252	0.33	0.29
$m_{ch}^{\perp}$	1.204	1.157	3.68	3.81	0.709	1.484	4.05	4.41
A_1	−4.789	−4.794	−3.95	−4.06	−4.367	−4.711	−3.86	−3.74
A_2	−0.550	−0.571	−0.27	−0.26	−0.518	−0.476	−0.25	−0.23
A_3	4.368	4.374	3.68	3.78	3.854	4.176	3.58	3.51
A_4	−1.511	−1.484	−1.84	−1.86	−1.549	−1.816	−1.32	−1.76
A_5	−1.734	−1.726	−1.95	−2.02	−1.680	−1.879	1.47	1.52
A_6	−1.816	−1.788	−2.91		−2.103	−2.355	1.64	1.83
A_7	0.134	0.153	0	0	0.204	0.096		0
Δ_1	−0.128	−0.160	−0.059	−0.059	−0.093	−0.093	−0.215	

[a] FPLAPW band-structure calculations from Ref. 50. Effective-mass parameters obtained through a 3D fitting procedure within cubic approximation.

[b] FPLAPW band-structure calculations from Ref. 50. Effective-mass parameters obtained by a direct line fit.

[c] A_i from Ref. 31 obtained through a Monte Carlo fitting procedure to the band structure and effective masses calculated using Eqs. (20) and (21).

[d] Direct $\mathbf{k}\cdot\mathbf{p}$ calculations for A_i from Ref. 31 and effective masses obtained from A_i using Eqs. (20) and (21).

[e] Direct fit of A_i to first-principles band-structures from Ref. 28.

[f] A_i and effective masses obtained in the quasicubic model from zinc-blende parameters from Ref. 28.

TABLE VIII. Effective masses in units of free electron mass m_0, Luttinger-like parameters A_i ($i=1,\ldots,6$) in units of $\hbar^2/2m_0$, and A_7 in units of eV Å for wurtzite phase GaN. The crystal-field splitting energy Δ_1 is given in units of meV.

Ref.	This work		[a]	[c]	[d]	[e]	[f]	[g]	[h]	[i]	[j]
	aniso	iso									
$m_e^{\parallel}$	0.138	0.138	0.20	0.20	0.14	0.14	0.19	0.19		0.19	0.19
$m_e^{\perp}$	0.151	0.151	0.18	0.18	0.15	0.15	0.17	0.17		0.23	0.19
$m_{hh}^{\parallel}$	2.000	2.007	1.10	1.76	1.479	1.453	1.76	1.96	1.89	2.00	1.96
$m_{lh}^{\parallel}$	2.000	2.007	1.10	1.76	1.479	1.453	1.76	1.96	1.89	2.00	1.96
$m_{ch}^{\parallel}$	0.130	0.130	0.15	0.16	0.130	0.125	0.14	0.14	0.12	0.16	0.16
$m_{hh}^{\perp}$	2.255	2.249	1.65	1.61	1.592	1.595	1.69	1.87	2.00	2.04	1.20
$m_{lh}^{\perp}$	0.191	0.261	0.15	0.14	0.299	0.236	0.14	0.14	0.15	0.18	0.16
$m_{ch}^{\perp}$	0.567	0.317	1.10	1.04	0.252	0.289	1.76	1.96	0.59	1.49	1.96
A_1	−7.692	−7.698	−6.56	−6.27	−7.706	−7.979	−7.14	−7.24	−7.21	−6.4	−6.36
A_2	−0.575	−0.600	−0.91	−0.96	−0.597	−0.581	−0.57	−0.51	−0.44	−0.50	−0.51
A_3	7.192	7.200	5.65	5.70	7.030	7.291	6.57	6.73	6.68	5.9	5.85
A_4	−2.855	−2.816	−2.83	−2.84	−3.076	−3.289	−3.30	−3.36	−3.46	−2.55	−2.92
A_5	−2.986	−2.971	−3.13	−3.18	−3.045	−3.243	−3.28	−3.35	−3.40	2.56	2.60
A_6	−3.360	−3.312	−4.86		−4.000	−4.281		−4.72	−4.9	3.06	3.21
A_7	0.160	0.171	[b]	[b]	0.194	0.179	0	0	0.094	0.108	0
Δ_1	0.043	0.023	0.039	0.038	0.022	0.022	0.021	0.021	0.021	0.036	

[a] FPLAPW band-structure calculations from Ref. 21. Effective-mass parameters obtained through a 3D fitting procedure within cubic approximation.

[b] A_7 in the range of 0.136 eV Å has been set to zero.

[c] FPLAPW band-structure calculations from Ref. 21. Effective-mass parameters obtained by direct line fit.

[d] A_i from Ref. 31 obtained through a Monte Carlo fitting procedure to the band structure and effective masses calculated using Eqs. (20) and (21).

[e] Direct $\mathbf{k}\cdot\mathbf{p}$ calculations for A_i from Ref. 31 and effective masses calculated using Eqs. (20) and (21).

[f] Effective-masses and A_i from Ref. 34 obtained through a line fit to the band structure.

[g] Direct $\mathbf{k}\cdot\mathbf{p}$ calculation in a 3D fit from Ref. 34.

[h] A_i obtained through a direct fit from Ref. 52 and effective masses calculated using Eqs. (20) and (21).

[i] Direct fit of A_i to first-principles band-structure calculations from Ref. 28.

[j] A_i and effective masses obtained in the quasicubic model from zinc-blende parameters from Ref. 28.

$$E_{2,3}=\tfrac{1}{2}(F'+K'+\lambda)\pm\tfrac{1}{2}\sqrt{(F'+K'-\lambda)^2+8H'^2}, \quad (18)$$

where "+" and "−" correspond to the E_2 and E_3 valence bands, respectively. F', K', and H' from Eq. (18) are defined by A_i as follows:

$$F'=\Delta_1+(A_1+A_3)k_z^2+(A_2+A_4)(k_x^2+k_y^2),$$

$$K'=A_5(k_x^2+k_y^2),$$

$$H'=\sqrt{(A_6^2k_z^2+A_7^2)(k_x^2+k_y^2)}. \quad (19)$$

As pointed out by Kim *et al.*,[28] assuming the A_7 parameter to be zero leads to a crossing of the crystal-field split-off band and the light-hole band near the Γ point in wurtzite crystals. However, the interaction of these two bands, which is described by the A_7 parameter and lifts the degeneracy at the crossing point, is allowed by symmetry and has absolutely to be included. Figure 8 shows the three highest-lying valence bands exemplary for the α-GaN band-structure calculation obtained via anisotropically screened model potentials, which can only be correctly fitted by means of Eq. (18) including the A_7 parameter.

The crystal-field splitting Δ_1 of GaN and InN is positive and therefore the effective masses of the three valence bands E_1, E_2, and E_3 correspond to heavy-hole, light-hole, and spin-orbit split-off-hole masses, respectively. On the other hand, for AlN, $\Delta_1<0$ and the effective masses of E_2 and E_3 correspond to the spin-orbit split-off-hole and light-hole mass, respectively. The hole masses $m^{\parallel}$ and $m^{\perp}$ are given in dependence on the Luttinger-like parameters A_i as follows. $m^{\parallel}$ along the k_z-direction ($k_x=k_y=0$):

$$m_0/m_{hh}^{\parallel}=-(A_1+A_3),$$

$$m_0/m_{lh}^{\parallel}=-(A_1+A_3),$$

$$m_0/m_{so}^{\parallel}=-A_1. \quad (20)$$

$m^{\perp}$ in the (k_x,k_y) plane ($k_z=0$):

TABLE IX. Effective-masses in units of free electron mass m_0, Luttinger-like parameters A_i ($i=1,\ldots,6$) in units of $\hbar^2/2m_0$, and A_7 in units of eV Å for wurtzite phase InN. The crystal-field splitting energy Δ_1 is given in units of meV.

Ref.	This work		a	b	c	d
	Aniso	Iso				
$m_e^{\parallel}$	0.138	0.137	0.11	0.11	0.10	0.10
$m_e^{\perp}$	0.141	0.140	0.10	0.10	0.10	0.10
$m_{hh}^{\parallel}$	2.438	2.493	1.56	1.67	1.431	1.350
$m_{lh}^{\parallel}$	2.438	2.493	1.56	1.67	1.431	1.350
$m_{ch}^{\parallel}$	0.140	0.137	0.10	0.10	0.106	0.092
$m_{hh}^{\perp}$	2.661	2.599	1.68	1.61	1.410	1.449
$m_{lh}^{\perp}$	0.148	0.157	0.11	0.11	0.196	0.165
$m_{ch}^{\perp}$	3.422	1.446	1.39	1.67	0.209	0.202
A_1	−7.156	−7.298	−9.62	−9.28	−9.470	−10.841
A_2	−0.244	−0.441	−0.72	−0.60	−0.641	−0.651
A_3	6.746	6.896	8.97	8.68	8.771	10.100
A_4	−3.340	−3.064	−4.22	−4.34	−4.332	−4.864
A_5	−3.208	−3.120	−4.35	−4.32	−4.264	−4.825
A_6	−4.303	−3.948		−6.08	−5.546	−6.556
A_7	0.072	0.103	0	0	0.278	0.283
Δ_1	0.214	0.084			0.0375	0.0375

[a]Effective-masses and A_i from Ref. 34 obtained through a line fit to the band structure.
[b]Direct $\mathbf{k}\cdot\mathbf{p}$ calculation in a 3D fit from Ref. 34.
[c]A_i from Ref. 31 obtained through a Monte Carlo fitting procedure to the band structure and effective masses calculated using Eqs. (20) and (21).
[d]Direct $\mathbf{k}\cdot\mathbf{p}$ calculations for A_i from Ref. 31 and effective masses calculated using Eqs. (20) and (21).

$$m_0/m_{hh}^{\perp} = -(A_2 + A_4 - A_5),$$

$$m_0/m_{lh}^{\perp} = -(A_2 + A_4 - A_5) - 2A_7^2/|\Delta_1|,$$

$$m_0/m_{so}^{\perp} = -A_2 + 2A_7^2/|\Delta_1|. \qquad (21)$$

The A_7 parameter strongly affects the effective masses. This can already be deduced from Eq. (21) or from Fig. 8. The influence of the different screening approaches is demonstrated in Figs. 8 and 9 that show the valence-band dispersion near the Γ point calculated by means of anisotropically/isotropically screened model potentials.

The results of the fitted effective masses using Eqs. (20) and (21) are given for AlN, GaN, and InN in Tables VII, VIII, and IX, respectively.

The results of our calculated electron effective masses $m_e^{\parallel}$ ($m_e^{\perp}$) 0.23 (0.24), 0.14 (0.15), and 0.14 (0.14) are in good agreement with the values 0.28 (0.32), 0.20 (0.20), and 0.12 (0.12) recommended by Vurgaftman *et al.*[19] for α-AlN, α-GaN, and α-InN, respectively. Also the crystal-field splitting energies −0.160, 0.023, and 0.084 obtained with isotropically screened model potentials quite well agree with the values −0.164, 0.019, and 0.041 given by Vurgaftman *et al.*[19] for α-AlN, α-GaN, and α-InN, respectively. The overestimation of crystal-field splitting energies obtained via band-structure calculations with anisotropically screened model potentials by at least a factor of 2 requires further investigations. In order to compare the influence of isotropical/anisotropical screening on the fitted model potential parameters, these two screening approaches will be dealt with in a further work where the model potential parameters are directly extracted from α-nitride and not from β-nitride experimental data.

IV. CONCLUSIONS

In the present work the electronic properties of the zinc-blende and wurtzite group-III nitride compound semiconductors AlN, GaN, and InN were studied within the EPM approach. The adjustable parameters r_i and z_i of the ionic model potentials were obtained from zinc-blende experimental data.

The calculated band-structures and the obtained sets of Luttinger parameters γ_i and direction-dependent effective masses of β-AlN, β-GaN, and β-InN are in agreement with other published results.

Exploiting the concept of transferable model potentials, we calculated the band-structure of the corresponding group-III nitrides in the wurtzite phase. It could be shown that the transfer of ionic model potential parameters from β- to α-nitrides gives reliable results for AlN and GaN. However, there is no good agreement of the calculated α-InN band structure with recently published experimental data of the fundamental transition energy. We, therefore, predict that the band gap of higher-quality β-InN samples will be at least 1.3 eV smaller than the experimental input data used for the fit of the cationic In model potential. Furthermore, we have demonstrated that the anisotropy of the wurtzite crystals can

easily be included in band-structure calculations via a direction-dependent screening of the ionic model potentials. Its influence on the band structure is the largest at the Γ point. For that reason the anisotropy of wurtzite group-III nitrides must be included when determining Γ point effective masses. Based on the calculated band-structures, we have derived complete sets of Luttinger-like parameters A_i and effective masses for α-AlN, α-GaN, and α-InN and demonstrated that the Luttinger-like parameter A_7 is of importance for the determination of the effective masses.

Finally, we want to point out that the reliability of the obtained results is basically founded on two facts. On the one hand, we use one and the same analytical expression for the description of the ionic model potentials for both α and β nitride crystal structures. The continuous description of the model potential in reciprocal space enables band-structure calculations where the model potential is required at many intermediate reciprocal lattice points. On the other hand we also successfully apply an analytical expression for the screening function $\varepsilon(q)$ which allows the incorporation of the wurtzite lattice anisotropy. This anisotropy mostly influences the Γ-point properties of the α-nitrides including the effective masses and the Luttinger-like parameters. We expect that our approach to the construction of reliable, continuous model potentials demonstrated here for the III-V-semiconductor constituents Al, Ga, In, and N, can also be adopted for constructing the model potentials for the constituents of the more ionic II-VI semiconductors. In addition to determining technologically relevant semiconductor bulk properties, the advantage of such transferable, continuous model potentials and an improved description of crystal specific anisotropies will become even more noticeable in demanding band-structure calculations, as, for example, for semiconductor random alloy materials, superlattices or quantum dots which possess large unit cells.

ACKNOWLEDGMENTS

We are grateful to G. Böhm for providing the EPM pseudopotential parameter code. This work was supported by Deutsche Forschungsgemeinschaft (Grant No. Gr1011/10-1).

[1] P.B. Perry and R.F. Rutz, Appl. Phys. Lett. **33**, 319 (1978).
[2] S. Loughin, R.H. French, W.Y. Ching, Y.N. Xu, and G.A. Slack, Appl. Phys. Lett. **63**, 1182 (1993).
[3] K.C. Zeng, J.Y. Lin, H.X. Jiang, and W. Yang, Appl. Phys. Lett. **74**, 3821 (1999).
[4] D.C. Reynolds, D.C. Look, W. Kim, Ö. Aktas, A. Botchkarev, A. Salvador, H. Morkoç, and D.N. Talwar, J. Appl. Phys. **80**, 594 (1996).
[5] K. Reimann, M. Steube, D. Fröhlich, and S.J. Clarke, J. Cryst. Growth **189/190**, 652 (1998).
[6] K. Osamura, K. Makajima, Y. Murakami, P.H. Shingu, and A. Ohtsuki, Solid State Commun. **11**, 617 (1972).
[7] N. Puychevrier and M. Menoret, Thin Solid Films **36**, 141 (1976).
[8] C.P. Foley and T.L. Tansley, Phys. Rev. B **33**, 1430 (1986).
[9] V.V. Mamutin, V.A. Vekshin, V.Y. Davydow, V.V. Ratnikov, T.V. Shubina, S.V. Ivanov, P.S. Kopev, M. Karlstein, U. Söderwall, and M. Willander, Phys. Status Solidi A **176**, 247 (1999).
[10] V.Y. Davydov, A.A. Klochikhin, R.P. Seisyan, V.V. Emtsev, S.V. Ivanov, F. Bechstedt, J. Furthmüller, H. Harima, A.V. Mudryi, J. Aderhold, O. Semchinova, and J. Graul, Phys. Status Solidi B **229**, R1 (2002).
[11] J. Wu, W. Walukiewicz, K.M. Yu, J.W. Ager III, E.E. Haller, H. Lu, W.J. Schaff, Y. Saito, and Y. Nanishi, Appl. Phys. Lett. **80**, 3967 (2002).
[12] T. Matsuoka, H. Okamoto, M. Nakao, H. Harima, and E. Kurimoto, Appl. Phys. Lett. **81**, 1246 (2002).
[13] S. Nakamura, M. Senoh, S. Nagahama, N. Iwasa, T. Yamada, T. Matsushita, H. Kiyoku, and Y. Sugimoto, Jpn. J. Appl. Phys., Part 2 **35**, L74 (1995).
[14] I. Akasaki, H. Amano, S. Sota, H. Sakai, T. Tanaka, and M. Koike, Jpn. J. Appl. Phys., Part 2 **34**, L1517 (1995).
[15] S. Nakamura, M. Senoh, S. Nagahama, N. Iwasa, T. Yamada, T. Matsushita, Y. Sugimoto, and H. Kiyoku, Appl. Phys. Lett. **70**, 868 (1997).
[16] S. Strite and H. Morkoç, J. Vac. Sci. Technol. B **10**, 1237 (1992).
[17] J.W. Orton and C.T. Foxon, Rep. Prog. Phys. **61**, 1 (1998).
[18] S.C. Jain, M. Willander, J. Narayan, and R. VanOverstraeten, J. Appl. Phys. **87**, 965 (2000).
[19] I. Vurgaftman, J.R. Meyer, and L.R. Ram-Mohan, J. Appl. Phys. **89**, 5815 (2001).
[20] W.J. Fan, M.F. Li, T.C. Chong, and J.B. Xia, J. Appl. Phys. **79**, 188 (1996).
[21] M. Suzuki, T. Uenoyama, and A. Yanase, Phys. Rev. B **52**, 8132 (1995).
[22] Z.H. Levine and St.G. Louie, Phys. Rev. B **25**, 6310 (1982).
[23] K. Kim, P.R.C. Kent, A. Zunger, and C.B. Geller, Phys. Rev. B **66**, 045208 (2002).
[24] T.K. Bergstresser and M.L. Cohen, Phys. Rev. **164**, 1069 (1967).
[25] L.E. Ramos, L.K. Teles, L.M.R. Scolfaro, J.L.P. Castineira, A.L. Rosa, and J.R. Leite, Phys. Rev. B **63**, 165210 (2001).
[26] M. Suzuki and T. Uenoyama, Jpn. J. Appl. Phys., Part 1 **34**, 3442 (1995).
[27] M.Z. Huang and W.Y. Ching, J. Phys. Chem. Solids **46**, 977 (1985).
[28] K. Kim, W.R.L. Lambrecht, B. Segall, and M.v. Schilfgaarde, Phys. Rev. B **56**, 7363 (1997).
[29] A. Rubio, J.L. Corkill, M.L. Cohen, E.L. Shirley, and St.G. Louie, Phys. Rev. B **48**, 11 810 (1993).
[30] M. Goano, E. Bellotti, E. Ghillino, G. Ghione, and K.F. Brennan, J. Appl. Phys. **88**, 6467 (2000).
[31] D.J. Dugdale, S. Brand, and R.A. Abram, Phys. Rev. B **61**, 12 933 (2000).
[32] S.K. Pugh, D.J. Dugdale, S. Brand, and R.A. Abram, J. Appl. Phys. **86**, 3768 (1999).
[33] J.-B. Xia, K.W. Cheah, X.-L. Wang, D.-Z. Sun, and M.-Y. Kong, Phys. Rev. B **59**, 10 119 (1999).
[34] Y.C. Yeo, T.C. Chong, and M.F. Li, J. Appl. Phys. **83**, 1429 (1998).

[35] W.J. Fan, M.F. Li, T.C. Chong, and J.B. Xia, Solid State Commun. **97**, 381 (1996).
[36] A. Tadjer, B. Abbar, M. Rezki, H. Aourag, and M. Certier, J. Phys. Chem. Solids **60**, 419 (1999).
[37] M. L. Cohen and J. R. Chelikowsky, *Electronic Structure and Optical Properties of Semiconductors* (Springer, Berlin, 1989).
[38] G. Böhm and K. Unger, Phys. Status Solidi B **216**, 961 (1999).
[39] I. Petrov, E. Mojab, R.C. Powell, J.E. Greene, J. Hultman, and J.-E. Sundgren, Appl. Phys. Lett. **60**, 2491 (1992).
[40] K. Tsubouchi and N. Mikoshiba, IEEE Trans. Sonics Ultrason. **32**, 634 (1985).
[41] M.P. Thompson, G.W. Auner, T.S. Zheleva, K.A. Jones, St.J. Simko, and J.N. Hilfiker, J. Appl. Phys. **89**, 3331 (2001).
[42] J. Šik, M. Schubert, G. Leibiger, V. Gottschalch, and G. Wagner, J. Appl. Phys. **89**, 294 (2001).
[43] T. Azuhata, T. Sota, K. Suzuki, and S. Nakamura, J. Phys. C **7**, L129 (1995).
[44] G. Ramírez-Flores, H. Navarro-Contreras, A. Lastras-Martínez, R.C. Powell, and J.E. Greene, Phys. Rev. B **50**, 8433 (1994).
[45] C.-Y. Yeh, Z.W. Lu, S. Froyen, and W. Zunger, Phys. Rev. B **46**, 10 086 (1992).
[46] J.A. Chisholm, D.W. Lewis, and P.D. Bristowe, J. Phys. C **11**, L235 (1999).
[47] G.L. Zhao, D. Bagayoko, and T.D. Williams, Phys. Rev. B **60**, 1563 (1999).
[48] *Numerical Data and Functional Relationships in Science and Technology*, edited by O. Madelung, M. Schulz, and H. Weiss, Landolt-Börnstein, New Series, Group III, Vol. 17, pt. a (Springer, New York, 1982).
[49] J.M. Luttinger and W. Kohn, Phys. Rev. **97**, 869 (1955).
[50] M. Suzuki and T. Uenoyama, Appl. Phys. Lett. **69**, 3378 (1996).
[51] M. Fanciulli, T. Lei, and T.D. Moustakas, Phys. Rev. B **48**, 15 144 (1993).
[52] G.B. Ren, Y.M. Liu, and P. Blood, Appl. Phys. Lett. **74**, 1117 (1999).